Inorg. Chem. **2007**, *46*, 5155–5165

Systematic Investigation of Trigonal-Bipyramidal Cyanide-Bridged Clusters of the First-Row Transition Metals

Mikhail Shatruk, Kristen E. Chambers, Andrey V. Prosvirin, and Kim R. Dunbar*

Department of Chemistry, Texas A&M University, College Station, Texas 77842-3012

Received September 27, 2006

Reactions between $[M'^{III}(CN)_6]^{3-}$ anions (M′ = Co, Cr, or Fe) and mononuclear complexes of M^{II} ions (M = Cr, Mn, Co, Ni, or Zn) produce a family of pentanuclear clusters $\{[M(tmphen)_2]_3[M'(CN)_6]_2\}$. The core of the clusters is formed by five metal ions that are bridged through six CN^- linkers into a trigonal bipyramid, with M and M′ ions occupying equatorial and axial positions of the bipyramid, respectively. Three of the CN^- ligands from each M′ center remain terminal and point toward the outside of the cluster, along the trigonal axes. Studies of magnetic coupling in the $\{[M(tmphen)_2]_3[Cr(CN)_6]_2\}$ family of clusters revealed a similarity between the observed magnetic exchange constants and the values estimated for the molecule-based magnets of the Prussian blue family. The type of the magnetic exchange varies across the series, changing from antiferromagnetic for M = Cr and Mn to ferromagnetic for M = Co and Ni. Complexes $\{[M(tmphen)_2]_3[Co(CN)_6]_2\}$, which contain diamagnetic Co^{III} ions in the axial positions, serve as convenient model compounds for an accurate assessment of the magnetic parameters for the equatorial M ions in the absence of magnetic interactions. The $\{[Co(tmphen)_2]_3[Cr(CN)_6]_2\}$ cluster exhibits cyanide linkage isomerism, the relative amount of which depends on the synthetic conditions.

Introduction

Cyanide chemistry quickly became one of the central topics of molecular magnetism in the mid-1990s after two independent research groups reported that analogues of the Prussian blue family exhibited remarkably high magnetic ordering temperatures,[1,2] the current record being eventually set at 376 K.[3] These findings, along with a topical review of cyanide chemistry[4] that appeared in 1997, spawned extensive research in this area, the result of which is a vast range of new compounds with unusual properties based on extended structures and molecular solids. In recent years, this period of rapid advancement in the chemistry of molecular cyanide compounds has culminated with the preparation of a number of complexes that behave as single-molecule magnets (SMMs)[5−11] or single-chain magnets (SCMs).[12−14]

The availability of cyanide-bridged clusters, in particular, has been invaluable for theoreticians working in the area of molecular magnetism, providing them with the simplest model systems for testing the proposed theories. The design of isomorphous families of simple clusters and the study of

* To whom correspondence should be addressed. E-mail: dunbar@mail.chem.tamu.edu.

(1) Mallah, T.; Thiebaut, S.; Verdaguer, M.; Veillet, P. *Science* **1993**, *262*, 1554−1557.
(2) Entley, W. R.; Girolami, G. S. *Science* **1995**, *268*, 397−400.
(3) Holmes, S. M.; Girolami, G. S. *J. Am. Chem. Soc.* **1999**, *121*, 5593−5594.
(4) Dunbar, K. R.; Heintz, R. A. *Prog. Inorg. Chem.* **1997**, *45*, 283−391.
(5) Sokol, J. J.; Hee, A. G.; Long, J. R. *J. Am. Chem. Soc.* **2002**, *124*, 7656−7657.
(6) Berlinguette, C. P.; Vaughn, D.; Cañada-Vilalta, C.; Galán-Mascarós, J. R.; Dunbar, K. R. *Angew. Chem., Int. Ed.* **2003**, *42*, 1523−1526.
(7) Choi, H. J.; Sokol, J. J.; Long, J. R. *Inorg. Chem.* **2004**, *43*, 1606−1608.
(8) Schelter, E. J.; Prosvirin, A. V.; Dunbar, K. R. *J. Am. Chem. Soc.* **2004**, *126*, 15004−15005.
(9) Wang, S.; Zuo, J. L.; Zhou, H. C.; Choi, H. J.; Ke, Y.; Long, J. R.; You, X. Z. *Angew. Chem., Int. Ed.* **2004**, *43*, 5940−5943.
(10) Li, D.; Parkin, S.; Wang, G.; Yee, G. T.; Prosvirin, A. V.; Holmes, S. M. *Inorg. Chem.* **2005**, *44*, 4903−4905.
(11) Wang, C. F.; Zuo, J. L.; Bartlett, B. M.; Song, Y.; Long, J. R.; You, X. Z. *J. Am. Chem. Soc.* **2006**, *128*, 7162−7163.
(12) Toma, L. M.; Lescouëzec, R.; Lloret, F.; Julve, M.; Vaissermann, J.; Verdaguer, M. *Chem. Commun.* **2003**, 1850−1851.
(13) Wang, S.; Zuo, J. L.; Gao, S.; Song, Y.; Zhou, H. C.; Zhang, Y. Z.; You, X. Z. *J. Am. Chem. Soc.* **2004**, *126*, 8900−8901.
(14) Toma, L. M.; Lescouëzec, R.; Pasán, J.; Ruiz-Pérez, C.; Vaissermann, J.; Cano, J.; Carrasco, R.; Wernsdorfer, W.; Lloret, F.; Julve, M. *J. Am. Chem. Soc.* **2006**, *128*, 4842−4853.

10.1021/ic061856t CCC: $37.00
Published on Web 02/28/2007

Scheme 1. Building a TBP Cluster from Mononuclear Components

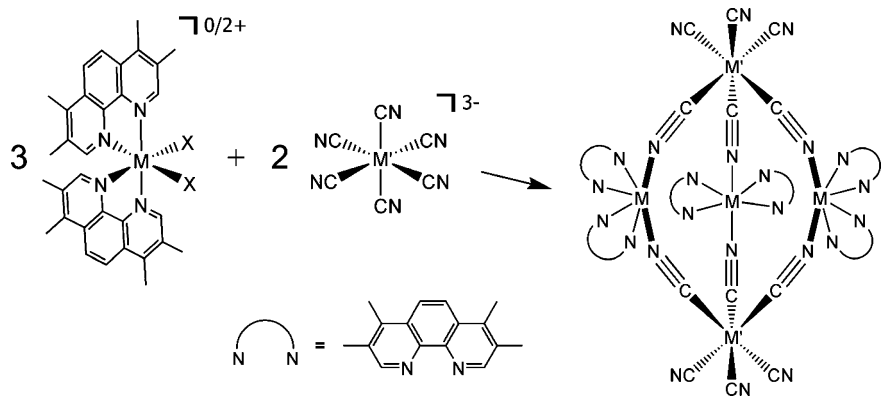

their magnetic properties is, therefore, one of the most important challenges for the advancement of molecular magnetism.[15−17]

Thus far, there have been relatively few *systematic* studies of cyanide-bridged clusters of transition metals restricted to a well-defined geometry.[18,19] By employing a building block approach (Scheme 1), we have focused on the preparation of trigonal-bipyramidal clusters from a strategy that involves reacting divergent hexacyanometallate anions $[M'(CN)_6]^{3-}$ with convergent precursors in the form of mononuclear transition metal complexes $[M(tmphen)_2X_2]^{0/2+}$ that possess two labile X ligands (X = Cl^-, Br^-, I^-, CH_3CN, CH_3OH, or other solvents; tmphen = 3,4,7,8-tetramethyl-1,10-phenanthroline). In earlier work in our laboratories, this synthetic approach led to the isolation of pentanuclear complexes $[Mn^{II}(tmphen)_2]_3[Mn^{III}(CN)_6]_2$[6] and $[Co^{II}(tmphen)_2]_3[Fe^{III}(CN)_6]_2$,[20,21] in which metal centers occupy vertices of the trigonal bipyramid (TBP) with cyanide bridges acting as edges of the bipyramid. These clusters exhibit the properties of single-molecule magnetism and charge-transfer-induced spin transition, respectively.

Herein, we describe the extension of this synthetic procedure to include other combinations of the first-row transition-metal ions, which provided a homologous series of new TBP clusters. The properties of these complexes are discussed and compared to the corresponding behavior of the related mixed-metal 3D Prussian blue materials.

Experimental Section

Physical Measurements. Infrared (IR) spectra were measured as Nujol mulls placed between KBr plates on a Nicolet 740 FTIR spectrometer. Magnetic measurements were performed on crushed polycrystalline samples with a Quantum Design SQUID magnetometer MPMS-XL. dc magnetic susceptibility measurements were carried out in an applied field of 1000 G over the temperature range of 2−300 K. Magnetization data were measured at 1.8 K with the magnetic field varying from 0 to 70 000 G. Reduced magnetization curves were collected in the 1.8−3.9 K temperature range in magnetic fields from 10 000 to 70 000 G. The data were corrected for diamagnetic contributions calculated from the Pascal constants.[22] Because of the high content of disordered solvent in the crystals of the compounds, each sample used for magnetic measurements was subjected to thermogravimetric analysis (TGA) immediately after the magnetic study in order to establish the correct molecular weight. The TGAs were performed on a Shimadzu TGA-50 thermogravimetric analyzer in the 298−573 K temperature range at a heating rate of 10 K/min.

Syntheses. $[M(tmphen)_2]_3[M'(CN)_6]_2 \cdot x$(solvent). In a typical preparation, a precursor of metal M was made in situ by combining 1 equiv of the metal salt with 2.0−2.5 equiv of tmphen in acetonitrile or methanol. The volume of solvent was adjusted to obtain a concentration of ∼4 mM with respect to metal M ion. Into 10 mL of this solution was poured an equal volume of a 4 mM solution of hexacyanometallate anion $[M'(CN)6]^{3-}$ in the same solvent, and the mixture was left to stand undisturbed for 2 to 3 days. After this period of time, X-ray-quality needlelike crystals were harvested by filtration, washed with copious quantities of solvent, and dried in vacuo. Table 1 lists the formulas and colors of the compounds as well as yields of the respective reactions. Detailed synthetic procedures for each compound are available as Supporting Information. To make it easier for the reader to follow the discussion, **1**−**11** will be referred to by number and by the short abbreviations given in Table 1.

X-ray Crystallography. General Procedures. In a typical experiment, a crystal selected for study was suspended in polybutene oil (Aldrich) and mounted on a cryoloop, which was placed in an N_2 cold stream. Single-crystal X-ray data were collected at 110, 120, or 150 K on a Bruker APEX or Bruker SMART 1000 diffractometer equipped with a CCD detector. The data sets were recorded as three ω-scans of 606 frames each, at 0.3° step width, and integrated with the Bruker SAINT[24] software package. The absorption correction (SADABS[25]) was based on fitting a function to the empirical transmission surface as sampled by multiple

(15) Mironov, V. S.; Chibotaru, L. F.; Ceulemans, A. *J. Am. Chem. Soc.* **2003**, *125*, 9750−9760.
(16) Tsukerblat, B. S.; Palii, A. V.; Ostrovsky, S. M.; Kunitsky, S. V.; Klokishner, S. I.; Dunbar, K. R. *J. Chem. Theory Comput.* **2005**, *1*, 668−673.
(17) Palii, A.; Ostrovsky, S. M.; Klokishner, S. I.; Tsukerblat, B. S.; Dunbar, K. R. *Chem. Phys. Chem.* **2006**, *7*, 871−879.
(18) Yang, J. Y.; Shores, M. P.; Sokol, J. J.; Long, J. R. *Inorg. Chem.* **2003**, *42*, 1403−1419.
(19) Marvaud, V.; Decroix, C.; Scuiller, A.; Guyard-Duhayon, C.; Vaissermann, J.; Gonnet, F.; Verdaguer, M. *Chem.—Eur. J.* **2003**, *9*, 1677−1691.
(20) Berlinguette, C. P.; Dragulescu-Andrasi, A.; Sieber, A.; Galán-Mascarós, J. R.; Güdel, H. U.; Achim, C.; Dunbar, K. R. *J. Am. Chem. Soc.* **2004**, *126*, 6222−6223.
(21) Berlinguette, C. P.; Dragulescu-Andrasi, A.; Sieber, A.; Güdel, H. U.; Achim, C.; Dunbar, K. R. *J. Am. Chem. Soc.* **2005**, *127*, 6766−6779.
(22) Carlin, R. L. *Magnetochemistry*; Springer-Verlag: Berlin, Germany, 1986.
(23) Shatruk, M.; Dragulescu-Andrasi, A.; Chambers, K. E.; Stoian, S. A.; Bominaar, E. L.; Achim, C.; Dunbar, K. R.; in preparation.
(24) *SMART and SAINT*; Siemens Analytical X-ray Instruments Inc.: Madison, WI, 1996.
(25) Sheldrick, G. M. *SADABS*; University of Gottingen: Gottingen, Germany, 1996.

Table 1. Molecular Formulas, Colors, Reaction Yields, and Abbreviations Used to Represent Compounds **1**−**11**

compound	molecular formula	abbreviation	color	yield (%)
1	$[Mn^{II}(tmphen)_2]_3[Co^{III}(CN)_6]_2$	Mn_3Co_2	pale yellow	33
2	$[CoII(tmphen)_2]_3[Co^{III}(CN)_6]_2$	Co_3Co_2	orange	83
3	$[Ni^{II}(tmphen)_2]_3[Co^{III}(CN)_6]_2$	Ni_3Co_2	purple	52
4	$[Zn^{II}(tmphen)_2]_3[Co^{III}(CN)_6]_2$	Zn_3Co_2	colorless	46
5	$[Cr^{II}(tmphen)_2]_3[Cr^{III}(CN)_6]_2$	Cr_3Cr_2	dark brown	35
6	$[Mn^{II}(tmphen)_2]_3[Cr^{III}(CN)_6]_2$	Mn_3Cr_2	pale yellow	33
7	$[Co^{II}(tmphen)_2]_3[Cr^{III}(CN)_6]_2$	Co_3Cr_2	peach/yellow[a]	36/39
8	$[Ni^{II}(tmphen)_2]_3[Cr^{III}(CN)_6]_2$	Ni_3Cr_2	pink	34
9	$[Mn^{II}(tmphen)_2]_3[Fe^{III}(CN)_6]_2$	Mn_3Fe_2	brown	32
10[b]	$[Zn^{II}(tmphen)_2]_3[Cr^{III}(CN)_6]_2$	Zn_3Cr_2		
11[b]	$[Zn^{II}(tmphen)_2]_3[Fe^{III}(CN)_6]_2$	Zn_3Fe_2		

[a] The color of samples of **7** is affected by cyanide linkage isomerism. [b] The preparation and properties of **10** and **11** are reported by us in another paper.[23] They are referred to in the current manuscript solely for the sake of comparison of their magnetic properties to the new compounds (vide infra).

equivalent measurements. Solution and refinement of the crystal structures was carried out using the SHELX[26] suite of programs and the graphical interface X-SEED.[27] Preliminary indexing of the data sets established similar monoclinic unit cells for all of the studied compounds. Systematic extinctions indicated the space group $P2_1/c$ (No. 14). All of the structures were solved by direct methods that resolved the positions of the metal atoms and most of the C and N atoms. The remaining non-hydrogen atoms were located by alternating cycles of least-squares refinements and difference Fourier maps. Hydrogen atoms were placed at calculated positions. A large number of interstitial solvent molecules were present in all of the structures. Most of these molecules are heavily disordered, and only for structures **2** and **9** was it possible to obtain a satisfactory model of the disorder. Given the fact that the refinement of the TBP clusters is essentially uninfluenced by the presence of the disordered solvents, the SQUEEZE routine[28] was applied to subtract the diffraction contribution from the disordered solvent and to evaluate the number of solvent molecules present in the interstices of **1**, **3**−**5**, **7**, and **8**. The final refinement was carried out with anisotropic thermal parameters for all non-hydrogen atoms of the TBP unit and isotropic thermal parameters for the disordered solvent molecules (the latter were refined only for **2** and **9**). A summary of pertinent information relating to unit cell parameters, data collection, and refinement statistics is provided in Table 2. Average bond distances around metal centers and bond angles of the M′−C≡N−M bridges are given in Table 3. Complete listings of bond distances and angles are available as Supporting Information.

All of the attempts to grow a single crystal of **6** of satisfactory quality to allow for an X-ray crystal structure determination were unsuccessful. Some crystals, however, were sufficiently large, allowing unit cell parameters to be obtained (primitive monoclinic cell with $a = 19.313(4)$, $b = 25.167(5)$, $c = 24.316(5)$ Å, $\beta = 99.42(3)°$), which confirmed that **6** is isostructural with the other structurally characterized compounds presented in this article.

Results and Discussion

Syntheses. The combination of a divergent hexacyanometallate anion $[M'(CN)_6]^{3-}$ with a convergent mononuclear precursor of an octahedral divalent 3d metal ion, in which four coordination sites are capped by two bis-chelating tmphen ligands, results in the precipitation of crystalline solids of the general formula $[M(tmphen)_2]_3[M'(CN)_6]_2 \cdot x$(solvent). The preparation method is general and was used to obtain TBP clusters for various combinations of the first-row transition-metal ions. The facile crystallization of pure samples of **1**−**11** is attributed to the fact that the clusters are neutral (they are essentially insoluble in most common solvents). One would expect that charged products based on the same starting materials would be much more soluble. The reaction is easily scaled up, as evidenced by the fact that preparations carried out on a 20-fold scale lead to yields comparable to those described in the Experimental Section. The products are air-stable and can be stored without specific precautions for prolonged periods of time. Of particular interest is the stability of **5** containing Cr^{II} ions, which are typically extremely air-sensitive. Obviously, the steric bulk afforded by the tmphen ligands around the perimeter of the molecule is excellent protection against oxidation of the Cr^{II} centers.

It should be noted that crystalline forms of **1**−**11** contain large and varying amounts of interstitial solvent as a result of the poor packing of the molecules. Examination of the compounds by TGA revealed that they gradually lose the interstitial solvent when heated to ∼120 °C. Above this temperature, the clusters remain stable to ∼250 °C, after which temperature they decompose with further heating.

Single-Crystal X-ray Structures. Single-crystal X-ray studies revealed that **1**−**11** are isostructural and crystallize in the monoclinic space group $P2_1/c$. The molecular structures consist of a pentanuclear core composed of CN-bridged M^{II} and M'^{III} ions (Figure 1a). The latter belong to $[M'(CN)_6]^{3-}$ moieties that occupy the axial positions of the TBP core. Three CN^- ligands of each hexacyanometallate unit act as bridges, and the other three terminal CN^- ligands point toward the exterior of the cluster. The three equatorial M ions are in pseudo-octahedral coordination environments that consist of two bidentate tmphen molecules and two bridging CN^- ligands. The tmphen ligands are involved in intra- and intermolecular $\pi-\pi$ interactions. Each tmphen ligand bound to the M(2) center engages in an intramolecular $\pi-\pi$ contact with a tmphen ligand from a neighboring M(1) or M(3) center (Figure 1b). In contrast, one tmphen ligand from the M(1) or M(3) center is involved in an intramolecular $\pi-\pi$ interaction with a tmphen ligand bound to the M(2) site, and

(26) Sheldrick, G. M. *SHELXS-97 and SHELXL-97*; University of Gottingen: Gottingen, Germany, 1997.
(27) Barbour, L. J. *J. Supramol. Chem.* **2001**, *1*, 189−191.
(28) Van der Sluis, P.; Spek, A. L. *Acta Crystallogr., Sect. A* **1990**, *46*, 194−201.

Table 2. Crystal Structural Data and Refinement Parameters for **1**−**5** and **7**−**9**

formula	$Mn_3Co_2N_{24}C_{108}H_{96}$ [**1**·13(CH_3CN)][a]	$Co_5N_{24}C_{108}H_{96}$ [**2**·7$^1/_4$(CH_3OH)·3$^3/_4$(H_2O)]	$Ni_3Co_2N_{24}C_{108}H_{96}$ [**3**·14(CH_3CN)][a]	$Zn_3Co_2N_{24}C_{108}H_{96}$ [**4**·21(CH_3CN)][a]
space group	$P2_1/c$ (No. 14)	$P2_1/c$ (No. 14)	$P2_1/c$ (No. 14)	$P2_1/c$ (No. 14)
unit cell	a = 19.449(2) Å	a = 19.494(2) Å	a = 19.225(2) Å	a = 19.348(5) Å
	b = 25.589(2) Å	b = 25.075(3) Å	b = 25.009(3) Å	b = 25.480(7) Å
	c = 25.047(2) Å	c = 24.727(3) Å	c = 24.716(3) Å	c = 25.186(7) Å
	β = 98.153(2)°	β = 98.979(2)°	β = 98.031(2)°	β = 97.888(4)°
unit cell volume, V	12 339(2) Å^3	11 939(2) Å^3	11 767(2) Å^3	12 299(6) Å^3
Z	4	4	4	4
density, ρ_{calc}	1.084 g/cm^3	1.233 g/cm^3	1.143 g/cm^3	1.104 g/cm^3
abs coeff, μ	0.611 mm^{-1}	0.746 mm^{-1}	0.799 mm^{-1}	0.890 mm^{-1}
crystal color and habit	colorless needle	orange needle	purple block	colorless needle
crystal size	1.20 × 0.16 × 0.16 mm^3	0.82 × 0.14 × 0.05 mm^3	0.50 × 0.31 × 0.15 mm^3	0.90 × 0.08 × 0.08 mm^3
temperature	150 K	150 K	150 K	150 K
radiation, λ	Mo Kα, 0.71073 Å	Mo Kα, 0.71073 Å	Mo Kα, 0.71073 Å	Mo Kα, 0.71073 Å
min. and max. θ	1.14 to 28.46°	1.06 to 26.37°	1.07 to 28.29°	1.33 to 26.37°
reflections collected	106 600 [R_{int} = 0.0550]	95 915 [R_{int} = 0.0855]	44 651 [R_{int} = 0.0519]	64 919 [R_{int} = 0.1772]
independent reflections	28 986	24 412	24 395	25 057
data/parameters/restraints	28 986/1258/0	24 413/1442/21	24 395/1259/0	25 057/708/30
R [$F_o > 4\sigma(F_o)$]	R_1 = 0.054	R_1 = 0.078	R_1 = 0.070	R_1 = 0.107
	wR_2 = 0.117	wR_2 = 0.218	wR_2 = 0.174	wR_2 = 0.215
GOF on F^2	1.054	1.029	0.820	1.014
max./min. residual densities, e·Å^{-3}	0.696, −0.273	0.891, −0.476	1.871, −0.574	1.162, −1.977

formula	$Cr_5N_{24}C_{108}H_{96}$ [**5**·18(CH_3CN)][a]	$Co_3Cr_2N_{24}C_{108}H_{96}$ [**7**·18(CH_3CN)][a]	$Ni_3Cr_2N_{24}C_{108}H_{96}$ [**8**·14.5(CH_3OH)][a]	$Mn_3Fe_2N_{24}C_{108}H_{96}$ [**9**·5.5(CH_3CN)·2.5(H_2O)]
space group	$P2_1/c$ (No. 14)	$P2_1/c$ (No. 14)	$P2_1/c$ (No. 14)	$P2_1/c$ (No. 14)
unit cell	a = 19.556(7) Å	a = 19.25(1) Å	a = 19.50(1) Å	a = 19.57(3) Å
	b = 25.089(8) Å	b = 25.35(1) Å	b = 25.12(2) Å	b = 25.36(4) Å
	c = 24.660(8) Å	c = 24.72(1) Å	c = 24.67(2) Å	c = 24.57(2) Å
	β = 97.151(7)°	β = 97.82(3)°	β = 98.17(3)°	β = 99.11(5)°
unit cell volume, V	12 005(7) Å^3	11 947(11) Å^3	11 962(16) Å^3	12 042(29) Å^3
Z	4	4	4	4
density, ρ_{calc}	1.101 g/cm^3	1.118 g/cm^3	1.116 g/cm^3	1.244 g/cm^3
abs coeff, μ	0.489 mm^{-1}	0.635 mm^{-1}	0.690 mm^{-1}	0.602 mm^{-1}
crystal color and habit	dark-brown needle	yellow needle	pink needle	yellow-brown needle
crystal size	0.52 × 0.13 × 0.02 mm^3	0.54 × 0.12 × 0.08 mm^3	0.50 × 0.09 × 0.06 mm^3	0.48 × 0.07 × 0.07 mm^3
temperature	110 K	120 K	110 K	120 K
radiation, λ	Mo Kα, 0.71073 Å	Mo Kα, 0.71073 Å	Mo Kα, 0.71073 Å	Mo Kα, 0.71073 Å
min and max θ	1.14 to 28.46°	1.07 to 23.26°	1.16 to 26.37°	1.05 to 26.37°
reflections collected	51 944 [R_{int} = 0.1647]	73 124 [R_{int} = 0.1931]	127 053 [R_{int} = 0.1327]	96 698 [R_{int} = 0.1500]
independent reflections	17 002	17 156	24 463	24 596
data/parameters/restraints	17 002/1223/0	17 156/1258/42	24 463/1258/0	24 596/1383/27
R [$F_o > 4\sigma(F_o)$]	R_1 = 0.122	R_1 = 0.089	R_1 = 0.069	R_1 = 0.099
	wR_2 = 0.274	wR_2 = 0.177	wR_2 = 0.135	wR_2 = 0.252
GOF on F^2	0.967	1.015	1.059	0.984
max/min residual densities, e·Å^{-3}	0.695, −0.605	0.388, −0.340	0.599, −0.340	1.138, −0.849

[a] The solvent content was estimated from the electron density attributed to the disordered solvent contribution by SQUEEZE.

the other tmphen ligand participates in an intermolecular $\pi-\pi$ interaction with a tmphen ligand from a neighboring cluster.

It should be noted that the three equatorial metal sites in the pentanuclear TBP molecule exhibit the same chirality (Δ or Λ). Nevertheless, the unit cell contains equal numbers of enantiomorphic $\Delta\Delta\Delta$ and $\Lambda\Lambda\Lambda$ molecules, which results in a centrosymmetric space group.

Infrared Spectroscopy. 1−**11** exhibit characteristic bands in the region of C≡N stretching frequencies. A comparison of the cluster IR data to the ν(C≡N) stretches observed for the extended Prussian blue phases and the free hexacyanometallate anions aids in the assignment of the bands in the new compounds to bridging or terminal CN^- ligands. As the data in Table 4 indicate, the IR spectra of **1**−**11** exhibit lower-frequency stretches that are only slightly shifted as compared to the corresponding modes of the $[M'(CN)_6]^{3-}$ ions and, therefore, are reasonably assigned to the terminal cyanides. Upon formation of the $M'^{III}-C\equiv N-M^{II}$ bridge, the CN stretching frequency increases as a result of kinematic coupling.[29] This is clearly reflected in the data for the PB materials, in which all cyanide ligands are bridging, with the exception of defective sites. **1**−**11** also exhibit higher-energy CN stretching vibrations that appear 20−60 cm^{-1} higher than the ν(C≡N) stretches of the free $[M'(CN)_6]^{3-}$ ions. These features are assigned to the bridging CN^- ligands.

It should be noted at this point that, in the case of the Co_3Cr_2 cluster (**7**), an additional feature is observed at 2103 cm^{-1} as a shoulder of the band corresponding to the terminal CN^- ligands. The presence of this stretch is suggestive of the occurrence of cyanide linkage isomerism upon flipping the CN^- ligand from the $Co^{II}-N\equiv C-Cr^{III}$ bridging mode to the $Co^{II}-C\equiv N-Cr^{III}$ configuration. As has been stated above, the formation of the cyanide bridge between two transition-metal ions should lead to an increase in the C≡N stretching frequency as compared to that of the original hexacyanometallate anion. This increase is simply due to the mechanical constraint on the motion of the CN group

(29) Bignozzi, C. A.; Argazzi, R.; Schoonover, J. R.; Gordon, K. C.; Dyer, R. B.; Scandola, F. *Inorg. Chem.* **1992**, *31*, 5260−5267.

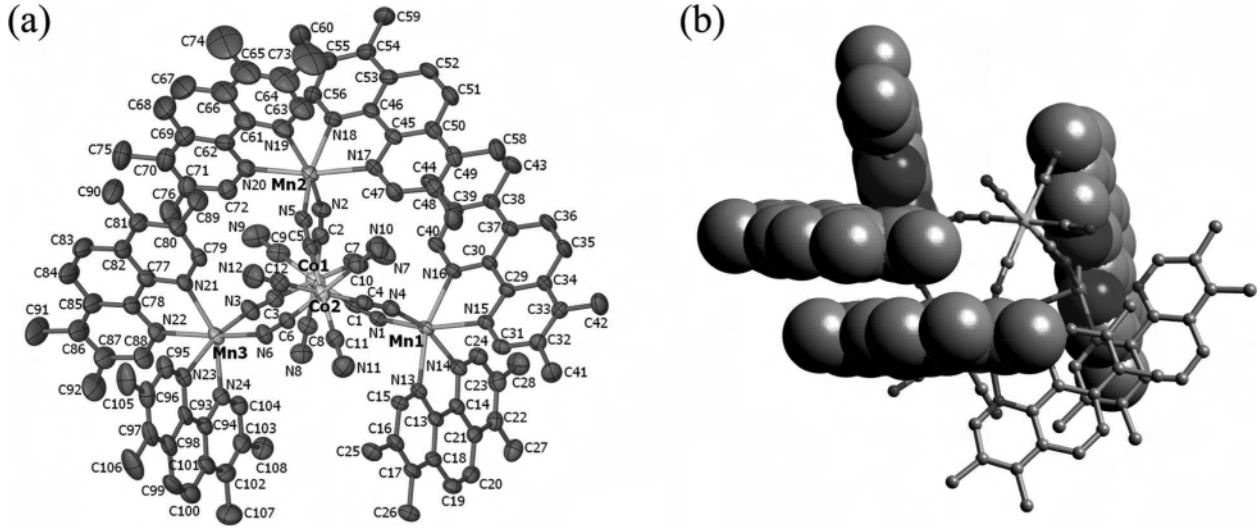

Figure 1. (a) Thermal ellipsoid plot of **1** (50% probability level; H atoms are omitted for clarity). (b) View of the TBP cluster in the crystal structure of **1** depicting one of the two intramolecular $\pi-\pi$ stacking interactions (horizontally arranged tmphen molecules) and the two tmphen ligands that do not participate in such an interaction (vertically arranged molecules).

Table 3. Average Metal-to-Ligand Bond Distances (Å) and Bond Angles (deg)[a] in the Crystal Structures of Compounds **1**−**5** and **7**−**9**

Mn_3Co_2 (**1**)				Co_3Co_2 (**2**)			
Mn(1)−N	2.245	Mn(1)−N≡C	163.3	Co(1)−N	2.125	Co(1)−N≡C	161.9
Mn(2)−N	2.233	Mn(2)−N≡C	160.1	Co(2)−N	2.123	Co(2)−N≡C	162.2
Mn(3)−N	2.233	Mn(3)−N≡C	161.3	Co(3)−N	2.131	Co(3)−N≡C	162.3
Co(1)−C	1.895	Co(1)−C≡N	176.8	Co(1′)−C	1.894	Co(1′)−C≡N	175.7
Co(2)−C	1.894	Co(2)−C≡N	176.9	Co(2′)−C	1.897	Co(2′)−C≡N	175.9
$C\equiv N_{bridging}$	1.145			$C\equiv N_{bridging}$	1.144		
$C\equiv N_{terminal}$	1.149			$C\equiv N_{terminal}$	1.147		
Ni_3Co_2 (**3**)				Zn_3Co_2 (**4**)			
Ni(1)−N	2.087	Ni(1)−N≡C	159.9	Zn(1)−N	2.158	Zn(1)−N≡C	161.8
Ni(2)−N	2.084	Ni(2)−N≡C	163.3	Zn(2)−N	2.140	Zn(2)−N≡C	159.8
Ni(3)−N	2.079	Ni(3)−N≡C	161.9	Zn(3)−N	2.157	Zn(3)−N≡C	160.2
Co(1)−C	1.898	Co(1)−C≡N	175.6	Co(1)−C	1.860	Co(1)−C≡N	176.6
Co(2)−C	1.894	Co(2)−C≡N	174.7	Co(2)−C	1.878	Co(2)−C≡N	177.3
$C\equiv N_{bridging}$	1.145			$C\equiv N_{bridging}$	1.181		
$C\equiv N_{terminal}$	1.153			$C\equiv N_{terminal}$	1.189		
Cr_3Cr_2 (**5**)				Co_3Cr_2 (**7**)[b]			
Cr(1)−N	2.027	Cr(1)−N≡C	167.9	Co(1)−N	2.099	Co(1)−N≡C	162.8
Cr(2)−N	2.027	Cr(2)−N≡C	166.6	Co(2)−N	2.088	Co(2)−N≡C	167.2
Cr(3)−N	2.031	Cr(3)−N≡C	164.8	Co(3)−N	2.089	Co(3)−N≡C	160.9
Cr(1′)−C	2.055	Cr(1′)−C≡N	171.9	Cr(1)−C	2.056	Cr(1)−C≡N	172.4
Cr(2′)−C	2.062	Cr(2′)−C≡N	172.2	Cr(2)−C	2.056	Cr(2)−C≡N	173.4
$C\equiv N_{bridging}$	1.160			$C\equiv N_{bridging}$	1.147		
$C\equiv N_{terminal}$	1.181			$C\equiv N_{terminal}$	1.177		
Ni_3Cr_2 (**8**)				Mn_3Fe_2 (**9**)			
Ni(1)−N	2.078	Ni(1)−N≡C	165.2	Mn(1)−N	2.225	Mn(1)−N≡C	162.0
Ni(2)−N	2.078	Ni(2)−N≡C	166.1	Mn(2)−N	2.234	Mn(2)−N≡C	160.8
Ni(3)−N	2.079	Ni(3)−N≡C	161.7	Mn(3)−N	2.242	Mn(3)−N≡C	164.7
Cr(1)−C	2.067	Cr(1)−C≡N	173.0	Fe(1)−C	1.919	Fe(1)−C≡N	176.4
Cr(2)−C	2.061	Cr(2)−C≡N	172.8	Fe(2)−C	1.927	Fe(2)−C≡N	176.9
$C\equiv N_{bridging}$	1.148			$C\equiv N_{bridging}$	1.151		
$C\equiv N_{terminal}$	1.138			$C\equiv N_{terminal}$	1.154		

[a] Only angles at bridging cyanides are given. [b] The refinement of the structure was performed without taking into account the cyanide linkage isomerism. All of the bridging cyanides were assumed to be of the Co−N≡C−Cr type.

generated by the presence of the second metal center (kinematic effect). Another important factor that determines the shift of $\nu(C\equiv N)$ is the π back-bonding from the metal d orbitals to the cyanide π^* orbitals. This effect is more pronounced at the C-bound metal center and results in lower C≡N stretching frequencies when the CN^- ligand is C-bound to an M^{II} ion rather than to an M^{III} ion. When a flip of the CN^- bridge occurs in the $Co^{II}{}_3Cr^{III}{}_2$ cluster, the C atom is

Table 4. IR Data in the ν(C≡N) Region (cm^{-1}) for Complexes **1**−**9**, the Corresponding PB Analogues, and the Free Hexacyanometallate Anions[a]

			ν(C≡N), cm^{-1}			
complex	M	M′	bridging	terminal	$[M'(CN)_6]^{3-}$ anion[b]	3D PB analogue
1	Mn^{II}	Co^{III}	2165, 2154, 2145	2131	2126	2160[30]
2	Co^{II}	Co^{III}	2167, 2157, 2148	2130, 2125	2126	2170[30]
3	Ni^{II}	Co^{III}	2174, 2164, 2154	2127, 2123	2126	2176[30]
4	Zn^{II}	Co^{III}	2173, 2164, 2155	2130	2126	2175[30]
5	Cr^{II}	Cr^{III}	2149	2126	2114	2194[1]
6	Mn^{II}	Cr^{III}	2153, 2144	2127	2114	2170[31]
7	Co^{II}	Cr^{III}	2155, 2147	2135, 2126 2103[c]	2114	2168[32]
8	Ni^{II}	Cr^{III}	2160, 2150	2127	2114	2150[33]
9	Mn^{II}	Fe^{III}	2147, 2141, 2135	2117, 2112	2101	2148[30]

[a] **1**−**9** contain varying amounts of interstitial solvent. The influence of these solvent molecules on the ν(C≡N) values is insignificant. [b] As measured for $(TEA)_3[Cr(CN)_6]$, $(TMA)_3[Fe(CN)_6]$, and $[(18\text{-crown-6})K]_3[Co(CN)_6]$ (TEA = tetraethylammonium, TMA = tetramethylammonium). [c] The appearance of this feature is attributed to cyanide linkage isomerism.

coordinated to the Co^{II} center, which leads to increased π back-bonding as compared to the case when the C atom is bound to the Cr^{III} ion. This situation leads to a ν(C≡N) decrease of ∼50 cm^{-1}.

The preparation of the Co_3Cr_2 cluster was perfomed in both methanol (**7b**) and acetonitrile (**7a**) solvents. When the reaction is carried out in methanol, an instantaneous precipitation of a peach-colored compound ensues after the reactants are mixed. It is interesting that the color of this product is similar to that of the $Co^{II}-Cr^{III}$ Prussian blue analogue obtained by fast precipitation of this material from aqueous solution.[34] Conversely, when the Co_3Cr_2 cluster is prepared in acetonitrile, the formation of the product occurs much more slowly, and the resulting compound is yellow. A comparison of the IR spectra of the two products revealed an increased quantity of the isomerized form of the cluster in **7a** prepared in acetonitrile (Figure 2). The IR of **7b** obtained from methanol does not show a discernible feature at 2103 cm^{-1}, but the presence of some small amount of the other isomer cannot be excluded, as determined by the magnetic behavior of the sample (vide infra).

Cyanide linkage isomerism was also reported for the $Co^{II}-Cr^{III}$ analogue of Prussian blue, but it was noted only when the compound was heated under an inert atmosphere.[34] In contrast, the transformation from the $Co^{II}-N\equiv C-Cr^{III}$ bridging mode to the $Co^{II}-C\equiv N-Cr^{III}$ isomer in molecular complex **7** is facilitated by the relatively slow formation of this cluster in acetonitrile solution. This opportune situation provides an ideal opportunity for a detailed investigation of the isomerization process by various spectroscopic techniques.[57]

Magnetic Properties. The dc magnetic properties of **1**−**3** and **5**−**9** were measured in the 2−300 K temperature range at an applied magnetic field of 1000 G. It is convenient to begin the discussion of magnetic properties with **1**−**3**. These clusters contain diamagnetic Co^{III} ions in the axial sites and, therefore, are used to determine the magnetic behavior of the paramagnetic metal centers in the equatorial positions of the TBP core independently. A precise determination of the characteristic magnetic parameters for the equatorial atoms can be applied to modeling the behavior of the magnetically coupled clusters containing axial Cr^{III} or Fe^{III} ions (**5**−**8** and **9**, respectively). Two other model compounds, namely **10** and **11**,[23] which contain diamagnetic Zn^{II} ions in the equatorial positions, serve to determine the magnetic behavior of the paramagnetic Cr^{III} and Fe^{III} ions, respectively, situated in the axial positions of the clusters.

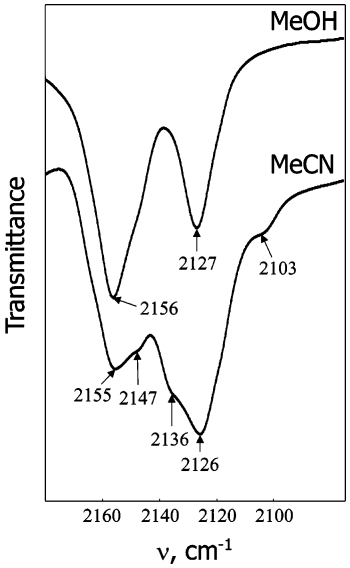

Figure 2. Cyanide stretches in the IR spectra of **7**, Co_3Cr_2, prepared in acetonitrile (MeCN, **7a**) and methanol (MeOH, **7b**).

$[M(tmphen)_2]_3[Co(CN)_6]_2$ (M = Mn (1), Co (2), or Ni (3)). For cluster **1**, Mn_3Co_2, the value of χT at 300 K is 13.1 emu·mol^{-1}·K, which corresponds well to the value of 13.13 cm^3·mol^{-1}·K expected for three isolated Mn^{II} ions ($S = {}^5/_2$, $g = 2.0$). The χT value is essentially constant over the entire temperature range from 300 to 2 K (Figure S1a), which indicates the absence of magnetic interactions between the equatorial Mn^{II} centers. An examination of the ground states for **1** was carried out by field-dependent magnetization measurements at 1.8 K. The data are in excellent agreement with the Brillouin function for three noninteracting $S = {}^5/_2$ ions (Figure S1b).

(30) Fernández, Bertrán J.; Reguera-Ruíz, E.; Blanco, Pascual J. *Spectrochim. Acta, Part A* **1990**, *46*, 1679−1682.
(31) Griebler, W. D.; Babel, D. *Z. Naturforsch., B* **1982**, *37B*, 832−837.
(32) Ohkoshi, S.; Hashimoto, K. *Chem. Phys. Lett.* **1999**, *314*, 210−214.
(33) Mallah, T.; Ferlay, S.; Auberger, C.; Helary, C.; L'Hermite, F.; Ouahes, R.; Vaissermann, J.; Verdaguer, M.; Veillet, P. *Mol. Cryst. Liq. Cryst., Sect. A* **1995**, *273*, 141−151.
(34) Brown, D. B.; Shriver, D. F. *Inorg. Chem.* **1969**, *8*, 37−42.

At 300 K, the value of χT for cluster **2**, $Co^{II}_3Co^{III}_2$, is 9.68 emu·mol^{-1}·K, which is much higher than the value expected for a spin-only case (5.625 emu·mol^{-1}·K for three isolated $S = {}^3/_2$ Co^{II} ions). This is easily understood by the fact that there are significant orbital contributions from the high-spin Co^{II} centers. The strong spin−orbit coupling combined with the crystal field distortion splits the $^4T_1$ term of the octahedral Co^{II} ion and stabilizes a ground-state Kramers doublet.[35] Therefore, as the temperature is lowered, the χT value is decreased as a result of the depopulation of the excited states and reaches a minimum of 6.0 emu·mol^{-1}·K at 2 K (Figure S1a). At low temperatures, each Co^{II} ion behaves as an effective $S' = {}^1/_2$ center. Field-dependent magnetization data collected at 1.8 K were fitted to the Brillouin function for three noninteracting Co^{II} centers with effective $S' = {}^1/_2$ and $g = 4.8$ (Figure S1b).

The room-temperature χT value for **3**, Ni_3Co_2, is 3.42 emu·mol^{-1}·K, which is slightly higher than the expected spin-only value of 3.00 emu·mol^{-1}·K for three isolated Ni^{II} ions, as expected for an orbital contribution. The value of χT remains constant over the entire temperature interval (Figure S1a). Field-dependent magnetization data measured at 1.8 K were fitted to the Brillouin function for three noninteracting Ni^{II} ions with $S = 1$ and $g = 2.08$ (Figure S1b). The absence of any appreciable zero-field splitting, typically observable for Ni^{II} complexes,[22] may be explained by the substantial distortion of the octahedral geometry caused by the bite angle of tmphen ligands or by cancellation of the individual zero-field contributions from Ni^{II} centers due to the high overall symmetry of the cluster.

It should be noted at this point that for **1** and **3** the χT value increases slightly at very low temperatures, which is suggestive of weak ferromagnetic coupling between the equatorial metal centers. This coupling would most likely be mediated by the diamagnetic Co^{III} ions in the axial sites of the TBP clusters. Such an interaction has been previously observed by Chen et al. for the trigonal bipyramidal cluster $[Ni(bpm)_2]_3[Co(CN)_6]_2$ (bpm = bis(1-pyrazolyl)methane),[36] in which equatorial Ni^{II} ions interact via N≡C−Co−C≡N bridges involving axial Co^{III} ions, but in the present case, the magnetic coupling is not as strong as reported by these authors (isotropic $J = 4.06$ cm^{-1}). This issue will be revisited in a following section in which the magnetic properties of cluster **8**, Ni_3Cr_2, are described.

$[M(tmphen)_2]_3[Cr(CN)_6]_2$ (M = Cr (5), Mn (6), Co (7), or Ni (8)). The magnetic behavior of these clusters differs significantly from that observed for **1**−**3** and is defined by magnetic exchange interactions between the equatorial M^{II} and axial Cr^{III} ions. Before discussing magnetically coupled clusters **5**−**8**, it should be mentioned that the magnetic behavior of model compound **10** (Zn_3Cr_2) is characteristic of two isolated Cr^{III} centers, with a χT value close to the spin-only value of 3.75 emu·mol^{-1}·K, which is nearly constant over the temperature range of 2−300 K (Figure S1a).[23]

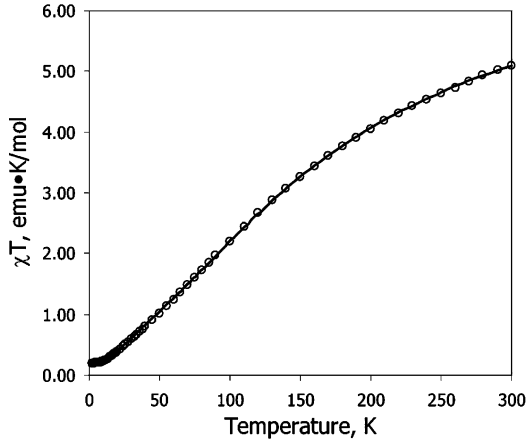

Figure 3. Plot of the temperature dependence of χT (○) for **5**, (Cr^{II}_3-Cr^{III}_2). The solid line corresponds to the Magpack simulation ($g_{Cr'} = 2.00$, $g_{Cr} = 2.32$, $J = -21.0$ cm^{-1}, $R2 = 0.9987$), which was carried out assuming the presence of a 2% Cr^{II} paramagnetic impurity.

$Cr^{II}_3Cr^{III}_2$. For **5**, $Cr^{II}_3Cr^{III}_2$, the value of χT at 300 K is 5.09 emu·mol^{-1}·K, which is considerably lower than the spin-only value of 6.75 emu·mol^{-1}·K expected for three low-spin Cr^{II} ions ($S = 1$) and two Cr^{III} ions ($S = {}^3/_2$) in the absence of magnetic coupling. The χT value continuously decreases and reaches a minimum of 0.2 emu·mol^{-1}·K at 2 K (Figure 3). The lower value of χT at room temperature and its decrease with temperature indicate significant antiferromagnetic coupling between Cr^{II} and Cr^{III} centers mediated by the cyanide bridges. To model the magnetic behavior, a spin Hamiltonian was used in the limit of an isotropic exchange interaction

$$H = -2J(S_{M1'} + S_{M2'})(S_{M1} + S_{M2} + S_{M3}) \qquad (1)$$

where J is the isotropic exchange constant and M′ and M correspond to the axial Cr^{III} and equatorial Cr^{II} ions, respectively. The simulation of the χT versus T curve was carried out using MAGPACK[37] and assuming $g_{Cr1'} = g_{Cr2'} = 2.00$ on the basis of the properties of the Zn_3Cr_2 cluster (**10**). The best simulation was obtained with $g = 2.32$ for the equatorial Cr^{II} ions and the exchange parameter $J = -21.0$ cm^{-1}.

Although Cr^{II}−Cr^{III} Prussian blue materials have been widely studied since the initial discovery of their high ordering temperatures,[1,38−40] there are few molecular complexes of Cr ions bridged by cyanide ligands. One unusual example is the compound $[(THF)_3Cr^{III}][(\mu\text{-}NC)Cr^0(CO)_5]_3$, in which Cr centers are present in mixed oxidation states. It was obtained in low yield as a byproduct of the reaction

(35) Abragam, A.; Pryce, M. H. L. *Proc. R. Soc. London* **1951**, *A206*, 173−191.
(36) Chen, X. Y.; Shi, W.; Xia, J.; Cheng, P.; Zhao, B.; Song, H. B.; Wang, H. G.; Yan, S. P.; Liao, D. Z.; Jiang, Z. H. *Inorg. Chem.* **2005**, *44*, 4263−4269.
(37) Borrás-Almenar, J. J.; Clemente-Juan, J. M.; Coronado, E.; Tsukerblat, B. S. *J. Comput. Chem.* **2001**, *22*, 985−991.
(38) Ohkoshi, S.-i.; Fujishima, A.; Hashimoto, K. *J. Am. Chem. Soc.* **1998**, *120*, 5349−5350.
(39) Vaucher, S.; Fielden, J.; Li, M.; Dujardin, E.; Mann, S. *Nano Lett.* **2002**, *2*, 225−229.
(40) Dostal, A.; Schroeder, U.; Scholz, F. *Inorg. Chem.* **1995**, *34*, 1711−1717.

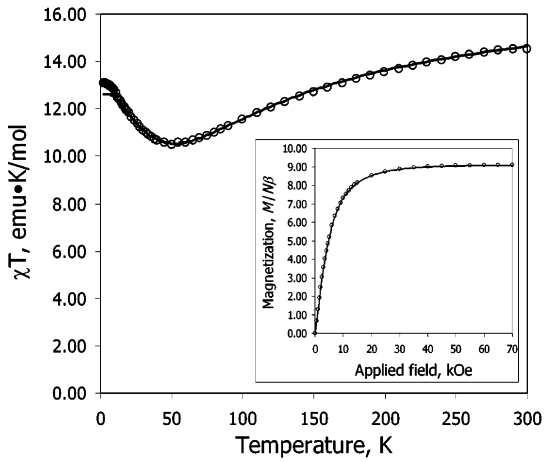

Figure 4. Temperature dependence of the χT product (○) for **6**, (Mn_3Cr_2). The solid line corresponds to the Magpack simulation ($g_{Cr} = g_{Mn} = 2.02$, $J = -4.7$ cm^{-1}, $R2 = 0.9980$). (Inset) Field-dependent magnetization at 1.8 K. The solid line corresponds to the best fit to the Brillouin function for $S = {}^9/_2$ ($g = 2.02$, $R2 = 0.9999$).

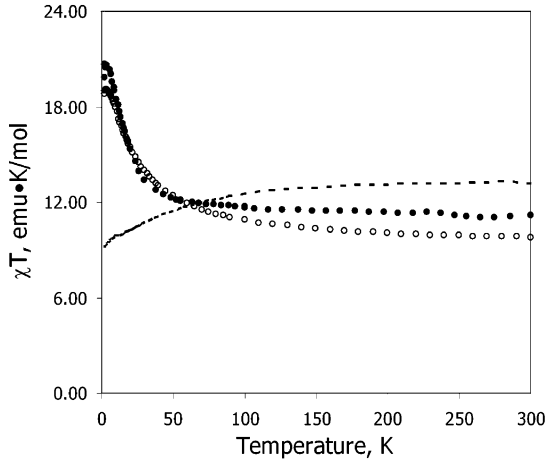

Figure 5. Temperature dependence of the χT product for samples **7a** (○) and **7b** (●) and the combined χT dependence for **2** and **10** (dashed line).

between $Na_2[Cr(CO)_5]$ and diisocyanotetrabromide.[41] Another example is the complex $(Ph_4P)[HO-Cr^{III}(cyclam)-NC-Cr^{III}(CN)_5]$, which was prepared by an elaborate synthetic procedure involving a mixture of mononuclear Cr^{III} complexes.[42] The only structurally characterized cyano-bridged complex of Cr^{II} has been recently reported by Miller's group: the molecule is the homoleptic $[Cr_2(CN)_9]^{5-}$ anion that cocrystallizes with the mononuclear $[Cr(CN)_5]^{3-}$ fragment.[43] The magnetic properties of the latter two mentioned dinuclear species revealed antiferromagnetic coupling with exchange constants of $J = -15.9$ and -13.3 cm^{-1}, respectively, which are comparable to the value of -21.0 cm^{-1} found for the present $Cr^{II}{}_3Cr^{III}{}_2$ cluster. To the best of our knowledge, cluster **5** represents the first successful attempt of the directed preparation of a cyano-bridged, mixed-valent molecular compound of Cr^{II}/Cr^{III}.

$Mn^{II}{}_3Cr^{III}{}_2$. The room-temperature χT value for **6**, Mn_3Cr_2, is 14.50 emu·mol^{-1}·K, which is less than expected for a spin-only case of uncoupled Mn^{II} ($S = {}^5/_2$) and Cr^{III} ($S = {}^3/_2$) ions ($\chi T = 16.88$ emu·mol^{-1}·K). The χT value continuously decreases from the value at room temperature and reaches a minimum of 10.50 emu·mol^{-1}·K at 50 K, indicating antiferromagnetic coupling between the Mn^{II} and Cr^{III} centers (Figure 4). Below 50 K, the χT value increases to reach a maximum of 13.08 emu·mol^{-1}·K at 2 K. The simulation of the χT versus T data was based on the Hamiltonian (eq 1), with M′ and M corresponding to the Cr^{III} and Mn^{II} ions, respectively. Assuming $g_{Cr} = g_{Mn} = g_{av} = 2.02$, the best agreement was achieved with the magnetic exchange constant $J = -4.7$ cm^{-1}. This value is comparable to the values of -6.2 and -3.1 cm^{-1} reported, respectively, for the trinuclear complex $\{[Cr^{III}(bpy)(CN)_4]_2[Mn^{II}(H_2O)_4]\}$ (bpy = 2,2′-bipyridine)[44] and the heptanuclear $Cr^{III}{}_6Mn^{II}$ cluster $K\{[Me_3tacnCr^{III}(CN)_3]_6Mn^{II}\}(ClO_4)_3$ (tacn = 1,4,7-triazacyclononane).[45] The maximum in the temperature dependence of χT is indicative of the stabilization of a high-spin ground state, which, according to the antiferromagnetic coupling scheme, is $S_{total} = 3S_{Mn} - 2S_{Cr} = {}^9/_2$. The Brillouin function calculated for $S_{total} = {}^9/_2$ and $g = 2.02$ fits well with the experimental data obtained by the measurement of the field-dependent magnetization at 1.8 K (Figure 4, inset).

$Co^{II}{}_3Cr^{III}{}_2$. As evidenced by the results of IR spectroscopy (vide supra), **7**, Co_3Cr_2, exhibits partial cyanide linkage isomerism. The transition from the $[(tmphen)_2Co(NC)_2]$ isomer to the $[(tmphen)_2Co(CN)_2]$ coordination mode is accompanied by a change in the ground-state spin of the Co^{II} center from high spin ($S = {}^3/_2$) to low spin ($S = {}^1/_2$). The high-spin state of the former fragment is confirmed by the properties of the $Co^{II}{}_3Co^{III}{}_2$ cluster (**2**), whereas the low-spin state of the latter can be anticipated from the strong-field nature of the carbon end of the cyanide ligand and is also in accord with the recent crystal structure determination of $Co(phen)_2(CN)_2$.[46] The change from the high-spin to low-spin state is expected to be reflected in the magnetic properties of bulk samples of the Co_3Cr_2 cluster. Indeed, as can be seen in Figure 5, cluster **7** shows different magnetic behavior depending on the method used to prepare the sample. When the compound is prepared in acetonitrile (sample **7a**), the χT value at 300 K is 9.75 emu·mol^{-1}·K, whereas for the sample prepared in methanol (**7b**), a value of 11.14 emu·mol^{-1}·K is observed. The CN flip in **7a** is indicated by the appearance of a band in the IR spectrum at 2103 cm^{-1}. Such a feature is not observed in the IR spectrum of **7b**, which implies that sample **7a** prepared in acetonitrile contains more of the isomer with the flipped CN^- groups.

The data in Figure 5 also depict a combined χT curve derived by adding the curves obtained for model clusters

(41) Edelmann, F.; Behrens, U. *J. Organomet. Chem.* **1977**, *131*, 65−72.
(42) Albores, P.; Slep, L. D.; Weyhermueller, T.; Rentschler, E.; Baraldo, L. M. *Dalton Trans.* **2006**, 948−954.
(43) Nelson, K. J.; Giles, I. D.; Shum, W. W.; Arif, A. M.; Miller, J. S. *Angew. Chem., Int. Ed.* **2005**, *44*, 3129−3132.
(44) Toma, L.; Lescouëzec, R.; Vaissermann, J.; Delgado, F. S.; Ruiz-Pérez, C.; Carrasco, R.; Cano, J.; Lloret, F.; Julve, M. *Chem.—Eur. J.* **2004**, *10*, 6130−6145.
(45) Heinrich, J. L.; Sokol, J. J.; Hee, A. G.; Long, J. R. *J. Solid State Chem.* **2001**, *159*, 293−301.
(46) Jian, F.; Xiao, H.; Li, L.; Sun, P. *J. Coord. Chem.* **2004**, *57*, 1131.

Scheme 2. Orbital Contributions to the Magnetic Superexchange via the CN− Ligand in Complexes **7a** and **7b**

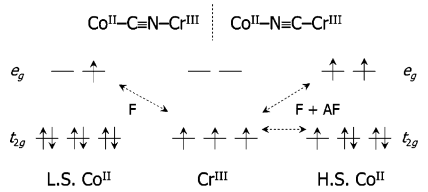

$Co^{II}_3Co^{III}_2$ (**2**) and $Zn^{II}_3Cr^{III}_2$ (**10**). The resulting χT temperature dependence corresponds to the magnetic behavior of a hypothetical unisomerized $Co^{II}_3Cr^{III}_2$ cluster in which the Co^{II} and Cr^{III} centers do not experience magnetic superexchange through the CN^- bridges and all of the CN^- bridges are C-bound to the axial Cr^{III} ions. In such a cluster, all of the Co^{II} ions would be in the high-spin electronic configuration state, which results in the total magnetic moment of this cluster being higher than the magnetic moments observed for either sample **7a** or **7b**. A comparison of this hypothetical curve to the experimentally measured data indicates that the Co^{II} and Cr^{III} ions are coupled ferromagnetically in both **7a** and **7b**. It is also evident that the coupling is stronger in the former case. This observation can be rationalized on the basis of a simple orbital consideration that takes into account that the major contributions to the magnetic superexchange via the M−N≡C−M′ bridge arise from the dπ−π overlaps between the t_{2g} orbitals of the metal ions and the π and π^* orbitals of the cyanide ligands.[47] Each overlap that involves t_{2g} orbitals with unpaired spins on both metal centers will provide an antiferromagnetic contribution to the total coupling. However, the interaction between unpaired spins located on a t_{2g} orbital of M and an e_g orbital of M′, or vice versa, will be ferromagnetic because the e_g orbital cannot overlap with the ligand π/π^* orbitals for symmetry reasons. We now apply this simple scheme to the case of the Co^{II}−C≡N−Cr^{III} versus Co^{II}−N≡C−Cr^{III} bridging mode (Scheme 2). In the former, the only unpaired electron on the Co^{II} center is located in an e_g obital, whereas the three unpaired electrons of the Cr^{III} ion occupy the t_{2g} orbitals. Because only ferromagnetic contributions are possible in this case, the resulting exchange interaction is essentially purely ferromagnetic. In the Co^{II}−N≡C−Cr^{III} bridging mode, the Co^{II} ions have one unpaired t_{2g} electron and two unpaired e_g electrons, which results in both antiferromagnetic and ferromagnetic contributions. Therefore, the ferromagnetic exchange should be more pronounced in the case of the Co^{II}−C≡N−Cr^{III} bridge. This is in agreement with the fact that the sample that contains a higher fraction of the cluster with flipped CN^- bridges, namely **7a**, exhibits a χT curve that increases faster than the curve for sample **7b**.

Samples **7a** and **7b** exhibit maxima in χT at 3.5 K of 19.1 and 20.6 emu·mol^{-1}·K, respectively (Figure 5), which indicate the stabilization of a ground state with a high-spin value. The Co^{II} ion in the $[(tmphen)_2Co(CN)_2]$ coordination environment is low-spin with $S_{Co} = {}^1/_2$. The Co^{II} ion in the $[(tmphen)_2Co(NC)_2]$ environment is high-spin with $S_{Co} = {}^3/_2$, but because of the strong spin−orbit coupling, the magnetic behavior of this ion at low temperature is an effective spin $S'_{Co} = {}^1/_2$, as in the case of cluster **2**, $Co^{II}_3Co^{III}_2$, whose magnetic properties were described in an earlier section. Nevertheless, the g factors used for the description of low-temperature magnetic properties in these two cases are very different. Typical g values for the low-spin Co^{II} ion are in the range of 2.2−2.4, whereas for the high-spin Co^{II} ion with an effective $S' = {}^1/_2$ ground state, the g values are typically higher than 4.[22] Because the content of the high-spin Co^{II} state is higher for the less isomerized sample (**7b**), the low-temperature maximum for this sample is observed at a higher value of χT.

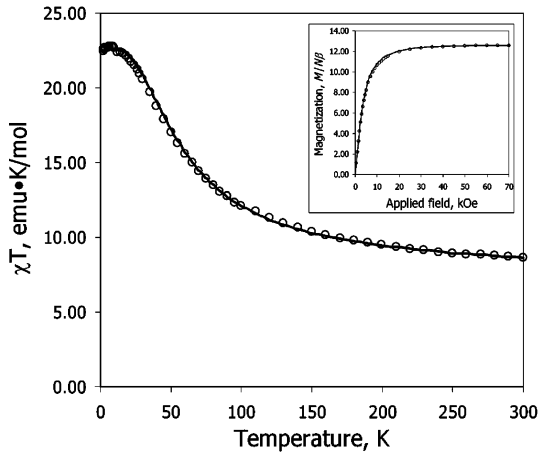

Figure 6. Temperature dependence of χT (○) for **8** (Ni_3Cr_2). The solid line corresponds to the Magpack simulation ($g_{Cr} = 2.00$, $g_{Ni} = 2.15$, $J = 8.5$ cm^{-1}, $R2 = 0.9989$). (Inset) Field-dependent magnetization at 1.8 K. The solid line corresponds to the best fit to the Brillouin function for $S = 6$ ($g = 2.10$, $R2 = 0.9994$).

The occurrence of cyanide linkage isomerism, along with the nontrivial magnetic behavior of high-spin Co^{II} ions, complicates the modeling of magnetic data for samples **7a** and **7b**. The consideration of magnetic exchange interactions and the spin states of Co^{II} centers as described above suggests that the Co^{II} and Cr^{III} ions in cluster **7** are ferromagnetically coupled. At low temperatures, this would lead to a stabilization of the ground state with $S_{total} = {}^9/_2$. We were able to fit the field-dependent magnetization data collected for sample **7a** at 1.8 K to the Brillouin function for the $S = {}^9/_2$ state, assuming $g = 2.48$ and an axial zero-field splitting parameter of $D = 0.5$ cm^{-1} (Figure S3). This fit, however, is only a rough approximation. To perform a more quantitative analysis of the magnetic data, we are currently pursuing the deliberate preparation of a TBP cluster in which the CN^- linkers are completely isomerized and all of the Co^{II} centers are in the low-spin electronic configuration.

$Ni^{II}_3Cr^{III}_2$. At 300 K, the value of χT for **8**, Ni_3Cr_2, is 8.64 emu·mol^{-1}·K, which is higher than expected for a spin-only case ($\chi T = 6.75$ emu·mol^{-1}·K). The χT value continuously increases from that at room temperature (Figure 6), indicating the existence of ferromagnetic coupling between Ni^{II} and Cr^{III} ions, which is expected given that the unpaired electrons are located on the e_g and t_{2g} orbitals, respectively. The MAGPACK simulation of the χT versus T data based on Hamiltonian (eq 1) with the parameter $g_{Cr} = 2.00$ led to $g_{Ni} = 2.15$ and the isotropic exchange constant $J = 8.5$ cm^{-1}.

(47) Weihe, H.; Güdel, H. U. *Comments Inorg. Chem.* **2000**, *22*, 75−103.

The latter is comparable to the values of 10.9 and 8.7 cm^{-1} reported for the linear $NiCr_2$ trimer in $\{[Ni(cyclam)][(Me_3tacn)Cr(CN)_3]_2\}(ClO_4)_2$ (cyclam = 1,4,8,11-tetraazacyclotetradecane, Me_3tacn = N,N′,N″-trimethyl-1,4,7-triazacyclononane)[48] and the heptanuclear $CrNi_6$ cluster in $\{[Ni(tetren)]_6[Cr(CN)_6]\}(ClO_4)_9$ (tetren = tetraethylenepentamine), respectively.[19] The value of χT reaches a maximum of 22.7 emu·mol^{-1}·K at 6 K, which is indicative of the stabilization of a high-spin ground state with $S = 6$. The field dependence of magnetization at 1.8 K was fitted to the Brillouin function for $S = 6$ and $g_{av} = 2.10$. (Figure 6, inset).

As mentioned in an earlier section, Chen et al. observed ferromagnetic coupling between Ni^{II} ions in trigonal bipyramidal cluster $[Ni(bpm)_2]_3[Co(CN)_6]_2$.[36] The isotropic exchange constant reported for this cluster is of the same order of magnitude as the one obtained in this work for the Ni_3Cr_2 cluster (**8**) (4.06 vs 8.5 cm^{-1}, respectively). In the former case, however, the magnetic coupling is mediated by long N≡C−Co−C≡N bridges that involve intermediary Co^{III} ions, in contrast to coupling via the much shorter C≡N pathway in **8**. We also observed ferromagnetic coupling in the analogous Ni_3Co_2 cluster (**3**) (Figure S1a), although it is weaker than in the case of the other two compounds. The observations of Chen et al. and our own observations led us to believe that the moderately strong ferromagnetic coupling that appears to be mediated by diamagnetic Co^{III} ions over a long pathway (which is an otherwise unprecedented type of situation) is likely to be an artifact caused by the presence of a magnetic impurity.

$[Mn(tmphen)_2]_3[Fe(CN)_6]_2$ (9). For **9**, Mn_3Fe_2, the value of χT at 300 K is 14.54 emu·mol^{-1}·K, which is slightly higher than the spin-only value of 13.88 emu·mol^{-1}·K expected for three high-spin Mn^{II} ($S = {}^5/_2$) and two low-spin Fe^{III} ($S = {}^1/_2$) ions in the absence of magnetic interactions. Nevertheless, this value compares favorably to the sum of the χT values for model clusters **1** (Mn_3Co_2) and **11** (Zn_3Fe_2). The deviation from the spin-only case is due to a significant orbital contribution that is well established for the $^2T_2$ ground state of the low-spin Fe^{III} ion[49−51] and confirmed by an examination of the model Zn_3Fe_2 cluster (Figure S1a).[23] The value of χT for **9** gradually decreases as the temperature is lowered (Figure 7) and reaches a minimum of 7.42 emu·mol^{-1}·K at 2 K, indicating antiferromagnetic coupling between the Mn^{II} and Fe^{III} ions. Antiferromagnetic exchange should result in a stabilization of the ground-state spin value of $S = {}^{13}/_2$. Given such a high-spin value, one would expect to observe a maximum of ∼24 emu·mol^{-1}·K in the low-temperature region of the χT plot, which is not the case for cluster **9**. The maximum magnetization value at 1.8 K and 7 T is 12.6μ_B, approaching the value of 13.0μ_B expected for the ground state $S = {}^{13}/_2$, (Figure 7, inset). The incomplete saturation suggests the presence of low-lying excited states that are populated even at low temperatures and high applied fields. An examination of field-dependent magnetization at different temperatures revealed that the Mn_3Fe_2 cluster is characterized by significant magnetic anisotropy (Figure S4). A thorough treatment of the magnetic behavior requires the application of more advanced physical models that are outside the scope of this article.

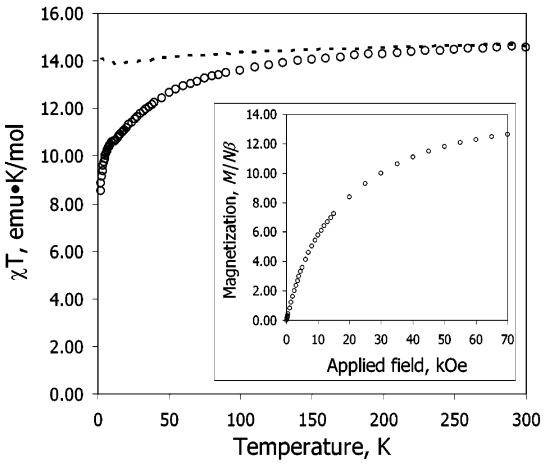

Figure 7. Temperature dependence of χT (○) for **9** and the combined χT dependence for **1** and **11** (dashed line). (Inset) Field-dependent magnetization at 1.8 K.

Magnetic Interactions in the TBP Clusters. The new TBP clusters represent simple assemblies of magnetically coupled transition-metal ions. With the exception of the Co_3Cr_2 (**7**) and Mn_3Fe_2 (**9**) clusters, whose magnetism is complicated by spin−orbit coupling and, in the former case, by cyanide linkage isomerism, the magnetic behavior of the compounds was interpreted straightforwardly by the use of the isotropic magnetic exchange Hamiltonian (eq 1). Model clusters M_3Co_2 (M = Mn (**1**), Co(**2**), Ni(**3**)) and $Zn_3M'_2$ (M′ = Cr (**10**), Fe (**11**)) were used for an accurate estimation of the individual ion magnetic parameters for use in modeling the magnetic properties of clusters **5**−**9**. The application of the isotropic exchange model to Cr_3Cr_2 (**5**), Mn_3Cr_2 (**6**), and Ni_3Cr_2 (**8**) resulted in J values of −21.0, −4.7, and +8.5 cm^{-1}, respectively. It is interesting to compare these values to the magnitude of the magnetic exchange interactions through the cyanide bridges in the Prussian blue-type solids. The latter can be estimated from the mean-field expression derived by Langevin, Weiss, and Néel[52]

$$T_C = \frac{2|J|}{3k_B}[xZ_M S_M(S_M + 1) \cdot Z_{M'} S_{M'}(S_{M'} + 1)]^{1/2} \qquad (2)$$

where S_M and $S_{M'}$ are spin values of individual M and M′ ions, Z_M and $Z_{M'}$ are the numbers of nearest metal centers connected to M and M′ via CN^- bridges, x is the stoichiometry of the PB-type compound, $M[M'(CN)_6]_x$, and k_B is the Boltzmann constant. The estimated J values for the PB materials (Table 5) are in good agreement with those found for molecular cyanide compounds **5**, **6**, and **8**, thereby supporting the hypothesis that these pentanuclear molecules serve as useful simple models for studying magnetic interactions in extended cyanide architectures. Molecular cyanide

(48) Berseth, P. A.; Sokol, J. J.; Shores, M. P.; Heinrich, J. L.; Long, J. R. *J. Am. Chem. Soc.* **2000**, *122*, 9655−9662.
(49) Figgis, B. N. *Trans. Faraday Soc.* **1961**, *57*, 198−203.
(50) Figgis, B. N. *Trans. Faraday Soc.* **1961**, *57*, 204−209.
(51) Baker, J.; Figgis, B. N. *Aust. J. Chem.* **1982**, *35*, 265−275.
(52) Neél, L. *Ann. Phys.* **1948**, *3*, 137−198.

Table 5. Magnetic Exchange Constants *J* Calculated for Clusters **5**, **6**, and **8** Using the Isotropic Exchange Hamiltonian (Equation 1) and Exchange Constants for Prussian Blue-Type Solids Estimated from Equation 2

cluster	J, cm^{-1}	PB type solid[a]	T_C, K	J, cm^{-1}
$Cr^{II}_3Cr^{III}_2$ (**5**)	−21.0	$Cr^{II}[Cr^{III}(CN)_6]_{0.67}$[1]	240	−22.8
$Mn^{II}_3Cr^{III}_2$ (**6**)	−4.7	$NaMn^{II}[Cr^{III}(CN)_6]$[54]	60	−1.8
$Ni^{II}_3Cr^{III}_2$ (**8**)	+8.5	$CsNi^{II}[Cr^{III}(CN)_6]$[56]	90	+5.7

[a] Formulas of the PB-type compounds also include interstitial and/or coordinated solvent molecules. For the sake of simplicity, these are not included in the formulas.

clusters provide the obvious advantage of being more readily crystallized than PB materials, which provides precise metrical parameters from the crystal structure determination. Moreover, in the few reported single-crystal structures, the PB materials are characterized by the presence of statistically disordered vacancies in the positions of the $[M'(CN)_6]^{n-}$ anions or the linkage disorder of the CN^- bridges, which leads to the description of the geometries around the metal centers as statistically averaged coordination environments.[53−55] The TBP clusters presented here do not exhibit any disorder with regard to both metal ions and CN^- ligands (with the exception of **7**) and allow for direct synthetic control over the identity of metal ions in equatorial and axial positions of the trigonal bypiramid.

Conclusions

A homologous family of new pentanuclear cyanide-bridged clusters based on the trigonal bipyramidal geometry was prepared and fully characterized by X-ray crystallography, infrared spectroscopy, and SQUID magnetometry. The magnitude of the exchange interactions between the transition-metal ions observed in these clusters correlates well with the values found for the respective mixed-metal Prussian blue-type phases that have been reported in the recent literature. The TBP clusters are excellent targets for advanced theoretical modeling of magnetically coupled systems because of their small size and relatively high symmetry. The Co_3Cr_2 cluster, **7**, exhibits cyanide linkage isomerism, with the extent of cyanide flipping being dependent on the solvent used in the preparation of the compound. The fact that the isomerization is quite slow in certain solvents bodes well for the process to be monitored by various spectroscopic techniques. These studies are in progress and will be reported in due course.

Acknowledgment. This research was supported by the NSF (PI grant CHE-0610019) and partially by the DOE (grant DE-FG03-02ER45999). Funding of the CCD diffractometer (CHE-9807975) by the NSF is gratefully acknowledged.

Supporting Information Available: Syntheses, additional details on magnetic properties, a listing of metal-to-ligand bond distances, and crystallographic files in CIF format. This material is available free of charge via the Internet at http://pubs.acs.org.

IC061856T

(53) Buser, H. J.; Schwarzenbach, D.; Petter, W.; Ludi, A. *Inorg. Chem.* **1977**, *16*, 2704−2710.
(54) Dong, W.; Zhu, L. N.; Song, H. B.; Liao, D. Z.; Jiang, Z. H.; Yan, S. P.; Cheng, P.; Gao, S. *Inorg. Chem.* **2004**, *43*, 2465−2467.
(55) Jiang, L.; Feng, X. L.; Lu, T. B.; Gao, S. *Inorg. Chem.* **2006**, *45*, 5018−5026.
(56) Gadet, V.; Mallah, T.; Castro, I.; Verdaguer, M.; Veillet, P. *J. Am. Chem. Soc.* **1992**, *114*, 9213−9214.
(57) The study of cyanide linkage isomerism in $Co^{II}-Cr^{III}$ cyanide-bridged complexes is currently in progress and will be reported in due course.